JACS
JOURNAL OF THE AMERICAN CHEMICAL SOCIETY

Article

pubs.acs.org/JACS

Dynamic Equilibria between Monomeric and Oligomeric Misfolded States of the Mammalian Prion Protein Measured by ^{19}F NMR

Sacha Thierry Larda,[†] Karen Simonetti,[‡] M. Sameer Al-Abdul-Wahid,[†] Simon Sharpe,*[,‡,§] and R. Scott Prosser*[,†,§]

[†]Department of Chemistry, University of Toronto, Toronto, Ontario, Canada M5S 3H6

[‡]Molecular Structure and Function Program, The Hospital for Sick Children, Toronto, Ontario, Canada M5G 1X8

[§]Department of Biochemistry, University of Toronto, Toronto, Ontario, Canada M5S 1A8

Supporting Information

ABSTRACT: The assembly of misfolded proteins is a critical step in the pathogenesis of amyloid and prion diseases, although the molecular mechanisms underlying this phenomenon are not completely understood. Here, we use ^{19}F NMR spectroscopy to examine the thermodynamic driving forces surrounding formation of β-sheet-rich oligomers early in the misfolding and aggregation pathway of the mammalian prion protein. We show that initial assembly of a small octameric intermediate is entropically driven, while further assembly to putative prefibrillar aggregates is driven by a favorable change in enthalpy. Kinetic data suggest that formation of the β-octamer represents a rate-limiting step in the assembly of prion aggregates. A disease-related mutation (F198S) known to destabilize the native state of PrP was also found to stabilize the β-octamer, suggesting that it can influence susceptibility to prion disease through two distinct mechanisms. This study provides new insight into the misfolding pathway leading to critical oligomers of the prion protein and suggests a physical basis for increased assembly of the F198S mutant.

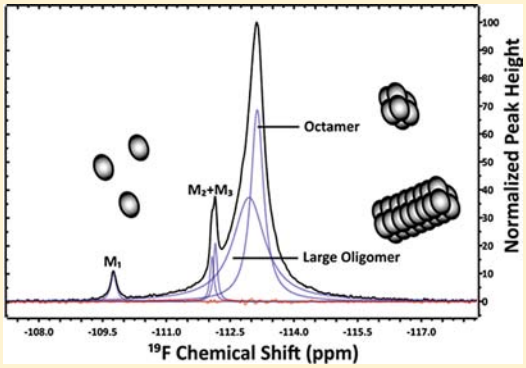

INTRODUCTION

A broad range of neurodegenerative diseases arise from the misfolding of endogenous proteins, leading to aggregation and protein deposition as amyloid fibril-rich deposits.[1,2] For example, misfolding of the mammalian prion protein (PrP) leads to the onset of Creutzfeldt−Jakob disease (CJD), Gerstmann−Straussler−Scheinker syndrome (GSS), fatal familial insomnia, and kuru in humans, as well as bovine spongiform encephalopathy in cattle, scrapie in sheep, and chronic wasting disease in deer and elk.[2−5] PrP is an endogenous glycosylphosphatidylinositol (GPI)-anchored protein associated largely with neuronal membranes, where it adopts a monomeric and predominantly α-helical structure in the nondiseased state (PrP^C).[6−8] Upon misfolding, which can occur sporadically in response to a destabilizing mutation, or through contact with its misfolded form (PrP^{Sc}), PrP converts to a β-sheet-rich, aggregation-prone state capable of forming a wide range of oligomeric structures, including the fibrillar form commonly associated with prion disease pathology.[9−13] While there is overwhelming evidence that misfolding and aggregation of PrP is the cause of both neuronal cell death and the infectious nature of prion diseases,[2,9,10,14,15] it is not yet clear exactly how cell death is induced or which oligomeric states of PrP are primarily responsible for disease pathogenesis.

In vitro, misfolding of PrP into a β-sheet-rich conformation can be initiated by high pressure, low pH, or addition of denaturant. In addition, hydrogen/deuterium (H/D) exchange data for PrP^C indicate the presence of residual structure in the unfolded state, within a region critical for pathological misfolding, suggesting that the process of PrP misfolding may proceed through unfolded intermediates in which regions containing defined structural elements are key to defining the PrP^C-to-PrP^{Sc} transition pathway.[16,17] Kinetic studies have indicated the presence of partially ordered monomeric intermediates populated during PrP folding or misfolding, although the dominant secondary structure observed is dependent on solution conditions.[18−21] There is also substantial evidence for the formation of several types of nonfibrillar, β-sheet-rich oligomers during the misfolding of PrP.[22−27] Recently, both *in vitro* and *in vivo* cytotoxicities have been demonstrated to arise primarily from nonfibrillar species,[9,25,28,29] rather than fibrils or monomeric protein. Similar cytotoxic nonfibrillar oligomers are also formed by the proteins implicated in several amyloid diseases and are suggested to be responsible for disease pathogenesis.[30−35]

Several distinct nonfibrillar oligomers have been reported to form during *in vitro* misfolding of PrP, ranging in size from 10 to 20 nm to over 50 nm in diameter. Octameric or decameric oligomers have been identified as the minimum stable assembly

Received: May 7, 2013
Published: June 20, 2013

   dx.doi.org/10.1021/ja404584s | J. Am. Chem. Soc. 2013, 135, 10533−10541

formed during PrP misfolding, and are typically reported as spherical or discoidal.[20−22,24−27,36−40] While there remains debate if these small oligomers exist on- or off-pathway to amyloid fibril formation, a recent study has linked a specific β-sheet-rich misfolding intermediate (the β-state) to prion disease susceptibility.[23] The β-state is an early misfolded state populated under conditions of low pH and mild denaturant and comprises β-sheet-rich oligomers in equilibrium with a small population of non-native monomers, reminiscent of the molten globule monomer−octamer equilibrium suggested by the work of Gerber et al.[21]

In order to develop a complete understanding of the mechanism of PrP misfolding and assembly, in particular the early events surrounding formation of an initial stable nucleus, it is important to elucidate the forces driving the oligomerization of PrP. To date, studies have primarily focused either on the thermodynamics and kinetics of PrP folding/unfolding,[18,19,41,42] or have tracked parameters associated with formation of oligomers from PrP^C.[22,26,36,38,43−45] In this paper, we examine the dynamic equilibrium that exists in the β-state misfolding intermediate between a non-native β-monomer, a stable β-octamer, and larger prefibrillar aggregates formed by the both wild type (WT) Syrian hamster PrP(90−231) (ShaPrP(90−231)) and an F198S mutant. The F198S mutation in humans is linked to familial prion disease (GSS), and destabilizes the native form of the protein, thus promoting misfolding.[18,41,46] ShaPrP(90−231) exhibits a high propensity to populate the β-state during unfolding, facilitating studies of this misfolding intermediate.[23] PrP(90−231) is also commonly used in studies of PrP misfolding, since residues 23−90 are inherently disordered in PrP^C and are not found within the protease-resistant core of PrP^{Sc}.[47−49] Importantly, β-state samples of PrP(90−231) have previously been shown to maintain a stable equilibrium, even at elevated temperatures, for a period of weeks.[23]

Herein, we make use of ^{19}F NMR to distinguish between assembled states present in β-state ShaPrP(90−231). ^{19}F is a highly sensitive NMR nucleus and exhibits a sizable chemical shift dispersion in response to changes in conformation or electrostatic environment.[50,51] Substitution of specific aromatic residues by their monofluorinated equivalents (in this case, 3-fluorophenylalanine) generally causes little or no structural perturbation.[52] By selectively introducing ^{19}F into either WT $PrP(90−231)^{\beta}$ or its F198S mutant, it is possible to spectroscopically quantify monomeric and oligomeric species coexisting within the β-state. The temperature and pressure dependence of the equilibrium then provides a thermodynamic perspective of the interactions which drive the formation of the octamer and prefibrillar states. In particular, enthalpy, entropy, and heat capacity differences between monomer, octamer, and prefibrillar aggregate states may be obtained by studying the equilibrium as a function of temperature, while pressure dependence provides information on specific volume and compressibility differences. At the same time, the equilibrium kinetics of exchange between states provides a perspective on the relative barriers involved in PrP oligomerization. This approach has allowed us to characterize early assembly events occurring during PrP misfolding. We distinguish the entropically favored formation of octamers from enthalpically driven assembly into larger species, and suggest that octamer formation from misfolded monomers is rate limiting. Additionally, an F198S mutation associated with GSS was shown to promote octamer formation, providing a new mechanism through which this mutation might lead to a pathogenic phenotype.

METHODS

Sample Preparation. Wild-type and F198S Syrian hamster PrP(90−231) were heterologously expressed in *E. coli*, using M9 minimal media enriched with $^{15}NH_4Cl$. Incorporation of 3-fluorophenylalanine was achieved through induced auxotrophy as described previously,[52] using 1 g/L glyphosate (to inhibit aromatic synthesis) and 75 mg/L of unlabeled tyrosine and tryptophan. When cells reached an OD of 0.8, 3-fluorophenylalanine was added at a concentration of 70 mg/L, and induced with 1 mM IPTG at 25 °C, overnight. Inclusion bodies were dissolved in 6 M guanidinium chloride (GuHCl), and His_6-tagged ShaPrP(90−231) was then purified by Ni^{2+} affinity chromatography. Refolding was achieved via rapid dilution into 55 mM Tris pH 8.2, 21 mM NaCl, 0.88 mM KCl, 1.1 M GuHCl, 400 mM L-arginine, 1 mM EDTA, 1 mM reduced glutathione, and 1 mM oxidized glutathione. Upon removal of the His-tag with TEV protease, natively structured PrP was converted to the β-state through dialysis in 10 mM sodium acetate pH 3.6, 150 mM NaCl, and 2 M urea for 48 h.[23] The F198S mutant was purified using a similar protocol, with thrombin for tag removal. Formation of the β-state was monitored using circular dichroism, and oligomeric β-state PrP was purified by gel filtration chromatography (Superdex 75). The equilibrium population of oligomer and β-state monomer was confirmed by gel filtration after incubation overnight. Samples were dialyzed into 10 mM sodium acetate, pH 3.6, concentrated, and doped with 7−8% D_2O for NMR.

NMR Experiments. All NMR experiments were performed on a 600 MHz (^1H Larmor frequency) Varian Inova spectrometer (Agilent Technologies, Santa Clara, CA) using a cryogenic 5 mm HCN probe, capable of being tuned to either ^1H or ^{19}F. Standard 90° pulse widths were 17.8−18.5 μs. All spectra were referenced to the internal lock. Generally, spectra were obtained using 4096 scans and a repetition time of 1.3 s. For variable-temperature studies, each experiment was separated by a 20-min equilibration period. The spectrum at 28 °C served as the reference for all deconvolutions, since it exhibited the largest M_1 peak intensity. Initial line width estimates at the reference temperature were derived from T_2-filtered diffusion experiments where the oligomer peak could be fit to a single line shape, indicating the elimination of the large oligomeric component. Initially, Lorentzian line widths were fixed, while peak heights and chemical shifts were optimized. Chemical shifts and peak intensities were then fixed, and line widths were then optimized in the deconvolution, as a function of temperature. Successive rounds of fitting were applied until changes in line width, shift, and intensity were minimal.

Saturation Transfer Experiments. An array of saturation pulses (0.03, 0.06, 0.2, 0.5, 0.7, 1.1, 1.4, 1.8 s for F198S and 0.03, 0.06, 0.1, 0.2, 0.5, 0.7, 1, 1.1, 1.4, 1.8 s for WT PrP), corresponding to a B_1 field of 14.3 kHz, was applied to the M_1 monomer peak (−108.9 ppm). An off-resonance saturation pulse was applied at the transmitter offset (−119 ppm), and its duration varied according to the on-resonance presaturation length in order to maintain a constant saturation period of 2 s. A control experiment was run with the saturation pulse at an equidistant frequency upfield from the oligomer peak; no saturation of the oligomer resonances was detected in the case of the control. The data was fit to a two-site exchange as described by Helgstrand et al.[53] A global fit was applied, allowing variation in $M(0)$, k, and T_1. T_1 was also separately measured using an inversion recovery experiment.

Pressure Experiments. 400 μL of WT or F198S $ShaPrP(90−231)^{\beta}$ at 3 mM were loaded into a ceramic high-pressure NMR tube pressurized using an Extreme-60 syringe pump (Daedalus Innovations). Light paraffin oil was used as the transducing fluid. Spectra were obtained as above, using 8192 scans. All pressure experiments were conducted at 28 °C. The sample was equilibrated for 20 min at each pressure prior to acquisition. Deconvolutions were conducted in a manner similar to that for the temperature experiments, using initial parameters derived from T_2-filtered diffusion experiments at 28 °C, 1 bar.

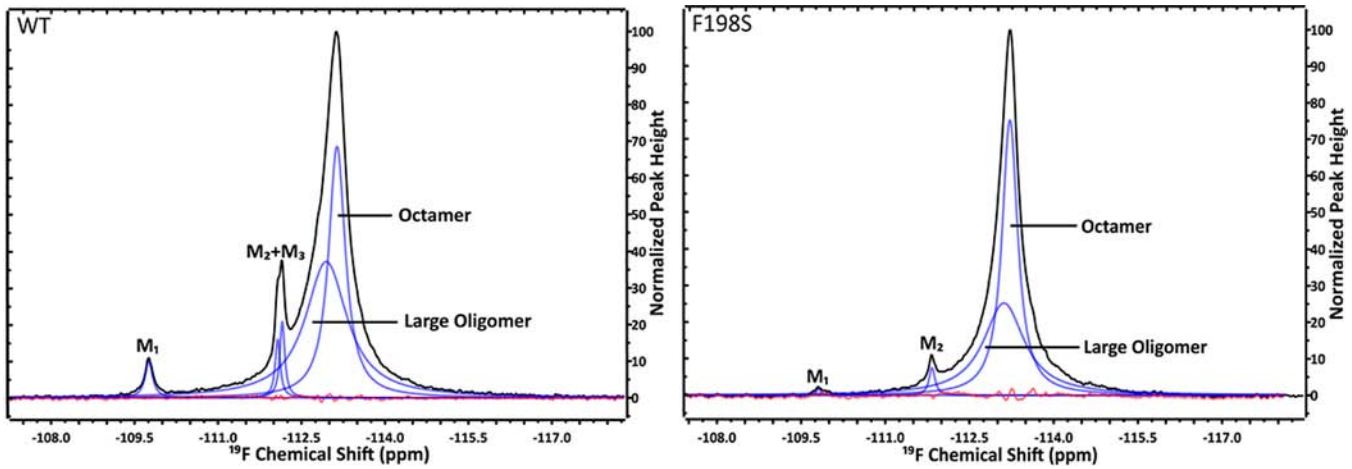

Figure 1. ^{19}F NMR spectra of 3-fluorophenylalanine-labeled ShaPrP(90−231)$^{\beta}$. Spectra (black lines) are shown for both WT (left) and F198S (right) samples containing 3 mM protein, 10 mM sodium acetate, pH 3.6, and 8% D_2O. The deconvolved peaks, shown in blue, are assigned the β-monomer (one for each 3-fluoro-Phe residue, designated as M_1, M_2, and M_3), β-octamer, and larger oligomers. Only two monomer peaks are observed for the F198S mutant, which lacks a third Phe residue. The residual error from peak fitting is shown in red. Spectra represent 4096 transients, obtained at 28 °C, at a 600 MHz ^{1}H field strength.

Diffusion Studies. A pulsed-gradient spin−echo ^{19}F diffusion experiment with variable gradient and t_1 mixing period (Δ) was employed. The gradient periods served as a T_2-filter which eliminated large oligomer intensity at values above 1 ms. Monomer and octamer line widths were estimated from an experiment with a gradient period of 1.5 ms and a t_1 mix time of 400 ms. The natural logarithm of normalized peak intensities were plotted as a function of $-\gamma^2G^2\delta^2(\Delta - (\delta/3)) \times D$ according to the Stejskal−Tanner equation,[54] and the apparent diffusion coefficient (D_{app}) of each species was determined from the slope of the plot. Similarly, an experiment was optimized for detection of large oligomer intensity. Due to exchange between states, the apparent diffusion coefficients were not suitable for quantitative analysis. Thus, the relative D_{app} values were used solely to support the assignment of monomer, octamer, and large oligomer resonances.

Thermodynamic Analysis. The equilibrium constant, k_{ij}, between two states, i and j, can be directly obtained from the ratio of corresponding peak areas in a one-dimensional ^{19}F NMR spectrum, assuming that states are not in intermediate or fast exchange with each other. The free energy associated with this equilibrium is given by

$$\Delta G_{ij} = -RT \ln k_{ij} \quad (1)$$

where R represents the gas constant. As it is difficult to obtain an accurate size for the higher-order aggregation states of PrP, we confine the present analysis to the use of effective equilibrium constants which do not specifically account for the aggregation number.[55] The temperature dependence of the free energy is in turn expressed in terms of the enthalpy, entropy, and heat capacity differences between the states, such that:[56]

$$\Delta G_{ij} = \Delta H_{ij} - T\Delta S_{ij} + \Delta C_{p,ij}[T - T_0 - T \ln(T/T_0)] \quad (2)$$

where T_0 refers to a reference temperature at which the enthalpy and entropy are defined. Assuming the enthalpy can be approximated as a constant over the full temperature range, the equilibrium constant can be expressed in terms of inverse temperature:

$$\ln k_{ij} = -\frac{\Delta H_{ij}}{RT} + \frac{\Delta S_{ij}}{R} \quad (3)$$

Similarly, the pressure dependence of the free energy provides a measure of the differences in both specific volume, ΔV_{ij}, and isothermal compressibility, $\Delta\kappa_{ij}$, between states:[56]

$$\Delta G_{ij} = \Delta G_0 + \Delta V_{ij}(P - P_0) - 0.5\Delta\kappa_{ij}(P - P_0)^2 \quad (4)$$

where ΔG_0 refers to the free energy difference at the reference temperature and pressure.

Dynamic Light Scattering. DLS experiments were performed using a 5 mm × 5 mm quartz cuvette in a PDDLS/Cool Batch 90T detector (Precision Detectors Inc., Bellingham, MA, U.S.A.). 300 μL aliquots of 20 μM β-state ShaPrP(90−231) in 10 mM sodium acetate pH 3.6 were used for all measurements. Precision Deconvolve32 software was used for data acquisition and analysis. Sampling time was 10 or 15 μs, and 10−12 scans were averaged for each data set. Scattering data were obtained at several temperatures between 20 and 80 °C, allowing the sample to equilibrate before each acquisition. Reversibility was confirmed by acquiring low-temperature data after each series. Literature values for viscosity were used for data analysis.

RESULTS

^{19}F NMR Spectra Reveal the Coexistence of β-Monomers, β-Octamers, and Higher-Order Oligomers. Samples of β-state ShaPrP(90−231) were prepared following previously reported protocols and their secondary structure and oligomeric state confirmed using gel filtration, DLS, and CD spectroscopy.[23] Figure 1 presents ^{19}F NMR spectra of WT and F198S ShaPrP(90−231)$^{\beta}$, labeled with 3-fluorophenylalanine. Previously reported gel filtration and sedimentation velocity data of PrP(90−231)$^{\beta}$ prepared at a lower concentration, using an otherwise identical sample preparation protocol, are consistent with the dominant species being octameric with only a small fraction of monomeric PrP present in the β-state.[23] Likewise, at temperatures below 60 °C, DLS measurements of our ShaPrP(90−231)$^{\beta}$ samples show a single dominant species corresponding to the expected hydrodynamic radius (∼6 nm) of an octamer (Figure S1 in Supporting Information [SI]). We therefore ascribe the well-resolved minor peaks in the ^{19}F NMR spectra to the non-native β-monomer for both WT and F198S ShaPrP(90−231). This assignment is supported by these resonances exhibiting longer T_2 relaxation times (Table S1 in SI) and faster NMR diffusion rates (Figure S2 in SI) than the broader peaks attributed to oligomeric PrP. The monomer resonances are designated M_1, M_2, and M_3 for WT PrP, corresponding to each of the fluoro-Phe residues (residues 139, 173, and 198) present in the WT sequence. While we cannot unambiguously assign F139 and F173, the absence of the M_3 peak in the spectrum of the F198S mutant allows us to assign that resonance to F198. Thus, only M_1 and M_2 are present in spectra of the F198S ShaPrP(90−231). F139 is expected to lie

dx.doi.org/10.1021/ja404584s | J. Am. Chem. Soc. 2013, 135, 10533−10541

within the disordered region of the protein, while both F173 and F198 are within ordered regions of both the native and fibrillar forms of PrP(90−231). Therefore, M_1 is likely to correspond to F139, while the two peaks with similar shifts correspond to F173 and F198. Note that site-specific assignment is not required for the present analysis of equilibrium populations of monomeric and oligomeric ShaPrP(90−231)$^{\beta}$. Rather, as long as each state can be spectroscopically resolved over a sufficient range of temperatures and pressures, the thermodynamic and volumetric parameters defining the differences between the states can then be determined, regardless of the location of the probe.

The upfield resonance associated with the β-state oligomer is significantly broader, such that each of the phenylalanine resonances appears equivalent, within the NMR line width. While the broad component of the ^{19}F spectrum was initially considered to arise solely from the β-octamer observed by DLS, spectral deconvolution reproducibly indicated the presence of two peaks, as shown in Figure 1. The ^{19}F spectrum cannot be accurately fit using a simple two-state (monomer−octamer) deconvolution. Moreover, both broad resonances are consistently observed over the entire temperature range of our NMR experiments (4−43 °C) and exhibit an inversely correlated change in intensity as a function of temperature. This suggests that these components represent an equilibrium between two distinct oligomeric states of PrP. NMR diffusion measurements, utilizing a ^{19}F NMR stimulated echo pulse sequence,[54,57] confirm that the broad resonances exhibit distinct diffusion rates, consistent with the presence of both an octamer and a larger oligomer (Figure S2 in SI). Furthermore, the component assigned to larger oligomers is completely abolished in Hahn-echo spectra with long delays to filter out fast-relaxing species, leaving only the longer-lived octamer and monomer peaks. Such T_2-filtered spectra can be fit with a single line shape to the octamer. As shown in Figure S1 in SI, DLS measurements obtained at elevated temperatures also show the reversible formation of a larger oligomeric species, consistent with the NMR diffusion data. The relatively small population of the larger oligomer seen by DLS can be attributed to those measurements being obtained at a concentration approximately 100 times lower than required for NMR.

Robust deconvolution of the ^{19}F NMR oligomer peak to obtain populations for the octamer and the larger oligomers relies on accurate estimates of the line widths for each component. In stimulated echo diffusion experiments with gradient duration longer than 1.5 ms, no large oligomer intensity could be detected, allowing determination of the octamer line width (Figure S2 in SI). These diffusion-filtered spectra provide reliable estimates of the line widths for both oligomeric species present in β-state PrP, allowing the accurate deconvolution of the ^{19}F spectra shown in Figure 1. T_2 relaxation (Hahn-echo) experiments also distinguish the octamer from the prefibril.[58] Using deconvolution of spectra obtained with varied echo times, and line width estimates from the T_2-filtered and diffusion-filtered spectra, it is possible to obtain T_2 relaxation times for each oligomeric species within the β-state, as reported in Table S1 in SI. The significantly shorter T_2 measured for the larger oligomer relative to octamer agrees with our assignment of these two species.

Thermodynamic Analysis of Monomer−Oligomer Equilibria of ShaPrP(90−231)$^{\beta}$. The identification of resolved resonances arising from β-state monomer and oligomeric PrP provides an opportunity to investigate the equilibria between these species as a function of temperature (16 - 43 °C) and pressure (1−1400 atm). Figure 2 shows the

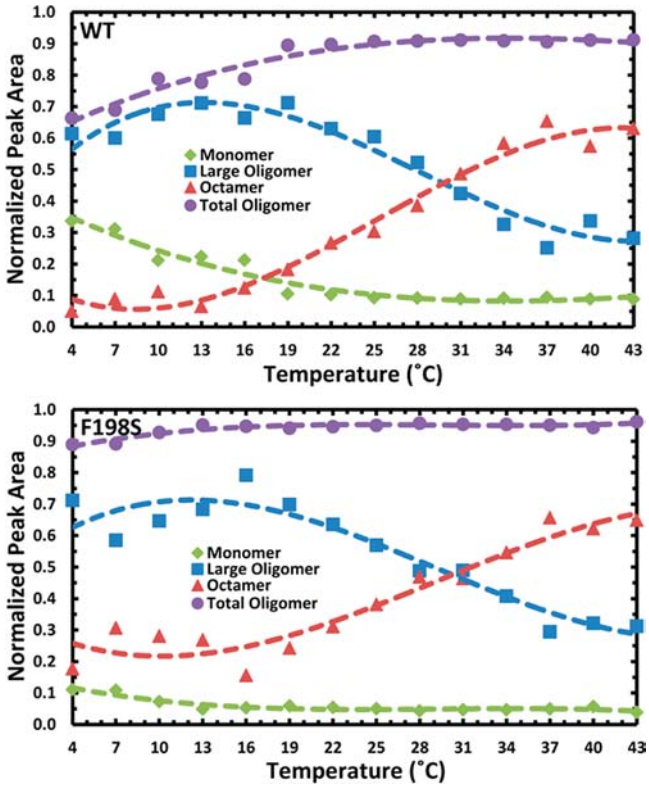

Figure 2. Equilibrium populations of β-state monomer, octamer, and large oligomers formed by ShaPrP(90−231) as a function of temperature. Relative normalized peak volumes were obtained from deconvolution of ^{19}F NMR spectra recorded at temperatures from 4−43 °C. The total oligomer fraction (calculated as the sum of the octamer and large oligomer populations) is also shown for both PrP sequences. In the case of F198S, the monomer profile was obtained by doubling the relative integral of the M_2 peak (the M_1 integral was unreliable as an estimate of the monomer population due to its broadened resonance). For the WT data, the monomer fraction was obtained using $(3/2)\times(M_2 + M_3)$ to obtain an estimate on the basis of the average over the two monomer peaks. Curves are shown to guide the eye.

temperature dependence of the β-monomer and oligomer fractions for WT and F198S ShaPrP(90−231)$^{\beta}$, based upon the relative normalized peak areas derived from spectral deconvolution. Monomer fractions remain very small over this temperature range but consistently decrease with temperature, with a corresponding increase in the total oligomer fraction. For both PrP sequences, temperatures above 31 °C favor the β-octamer, whereas lower temperatures favor the larger oligomers. Given the overlap between the broadened resonances corresponding to octamer and large oligomers, we have performed the analysis in two ways: 1) two-states, considering only the monomer and total oligomer (the sum of octamer and larger oligomer), and 2) three-states, where we distinguish monomer, octamer and larger oligomer based upon spectral deconvolution. In either case, the ratios of any two states directly relates to the free energy difference between states. By making use of eq 2, it is possible to then fit the temperature dependence of the resulting free energy terms (Figure 3), thereby providing an estimate of the enthalpy, entropy, and heat capacity differences between monomer and

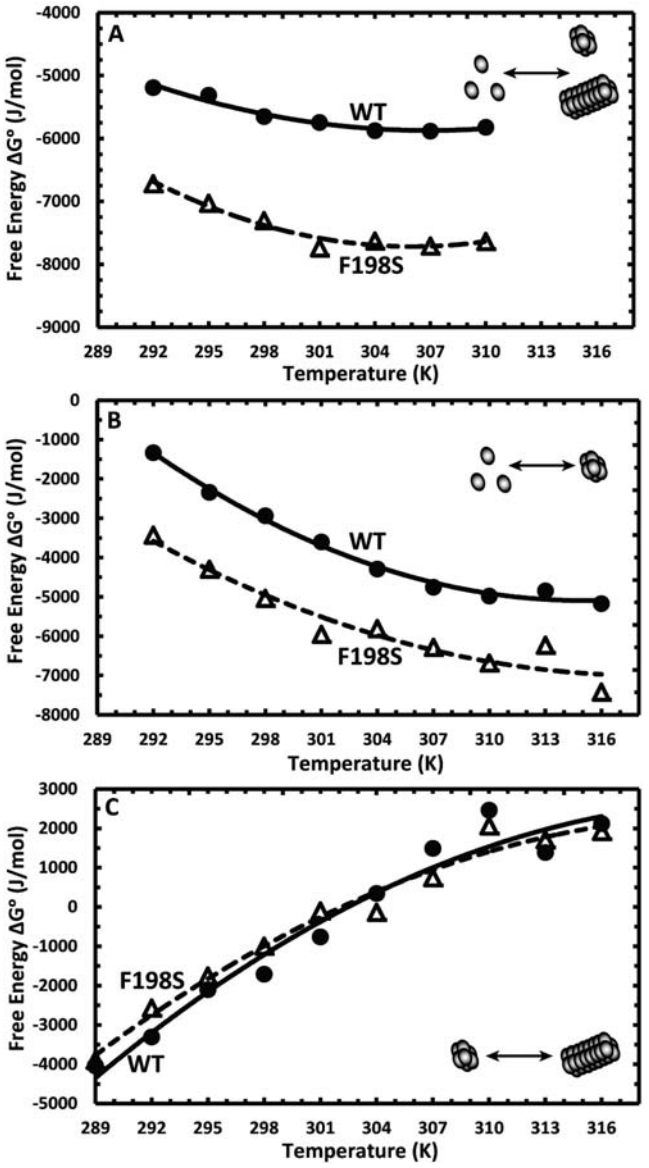

Figure 3. Free energy (ΔG) of association between β-state components as a function of temperature for WT (●) and F198S ShaPrP(90−231) (△). Free energy differences, as a function of temperature, are shown for the monomer to total oligomer (A), monomer to octamer (B), and octamer to large oligomer transitions (C). The data were fit using eq 2.

oligomer (octamer or large oligomer) or between β-octamer and large oligomer.

The results of the thermodynamic analysis, shown in Table 1, reveal that the formation of oligomeric species from monomer is strongly driven by entropy, while the enthalpy change associated with this initial aggregation step is unfavorable. The favorable entropic term for oligomerization presumably arises from burial of hydrophobic residues and decreased hydration of misfolded PrP upon formation of the octamer. On the other hand, equilibrium data associated with the transition between octamers and larger oligomers suggests a process that is entropically unfavorable although strongly enthalpically favorable. As shown in A and B of Figure 3, the F198S mutant exhibits significantly lower ΔG values associated with oligomer formation from monomeric protein. This mutation appears to favor the monomer−octamer transition, whereas little difference is seen for subsequent assembly of octamers into larger oligomers (Figure 3C).

Table 1. Thermodynamic Parameters Associated with the Temperature-Induced Transition from Monomer to Oligomer and Octamer to Large Oligomer for WT and F198S PrP(90−231)$^{\beta a}$

monomer to total oligomer (WT)		monomer to total oligomer (F198S)	
ΔH (kJ/mol)	5.83 ± 1.15	ΔH (kJ/mol)	8.83 ± 1.98
ΔS (J/mol/K)	40.00 ± 4.00	ΔS (J/mol/K)	50.00 ± 6.00
ΔC_p (kJ/mol/K)	−2.00 ± 0.40	ΔC_p (kJ/mol/K)	−3.20 ± 0.71
monomer to octamer (WT)		monomer to octamer (F198S)	
ΔH (kJ/mol)	55.00 ± 2.30	ΔH (kJ/mol)	45.70 ± 6.42
ΔS (J/mol/K)	198.00 ± 7.55	ΔS (J/mol/K)	170.10 ± 21.46
ΔC_p (kJ/mol/K)	−4.30 ± 0.51	ΔC_p (kJ/mol/K)	−2.97 ± 1.45
octamer to large oligomer (WT)		octamer to large oligomer (F198S)	
ΔH (kJ/mol)	−75.50 ± 7.17	ΔH (kJ/mol)	−65.50 ± 5.53
ΔS (J/mol/K)	−250 ± 24.00	ΔS (J/mol/K)	−220 ± 18.00

[a]Changes in enthalpy (ΔH), entropy (ΔS), and heat capacity (ΔC_p) are reported. In the three-state model, formation of the large oligomer (from octamer) did not show a change in heat capacity (no second-order term is present when fitting the temperature-dependent free energy profile of this transition).

Pressure-Induced Changes in Specific Volume and Isothermal Compressibility for the Monomer−Oligomer and Octamer−Large Oligomer Transitions of ShaPrP(90−231)$^{\beta}$. The equilibrium between β-state PrP monomers and oligomers was also studied as a function of pressure. The monomer, octamer, large oligomer, and total oligomer fractions were obtained through deconvolution of ^{19}F NMR spectra acquired at pressures from 1 to 1400 atm. As shown in Figure 4, WT ShaPrP(90−231)$^{\beta}$ exhibits a reduction in total oligomer as pressure is increased, with a concurrent increase in the monomer population. Similarly, there is an apparent pressure-induced dissociation of the large oligomers, leading to an increase in octamer. Similar analysis of the F198S β-state revealed a significantly weaker dependence of oligomerization on pressure, preventing accurate determination of free energies of association for the mutant protein.

The free energies calculated for the pressure-induced monomer−total oligomer and octamer−large oligomer transitions of WT ShaPrP(90−231)$^{\beta}$ are provided in Figure 5. The changes in partial specific volume (ΔV) and isothermal compressibility (ΔK_m) for each transition were obtained using eq 4 (Table S2 in SI). While compressibility was largely unaffected, the negative value for ΔV indicates that the system undergoes a collapse upon formation of oligomers from monomers, consistent with burial of hydrophobic surface suggested by the favorable entropy of this event. On the other hand, formation of large oligomers from octameric ShaPrP(90−231) is associated with a positive change in specific volume, possibly due to conformational rearrangements accompanying further assembly.

Exchange of ShaPrP(90−231) between β-Monomer and Oligomer States Occurs on a Time Scale of 4−10 s. The chemical shift separation between one of the β-monomer resonances (M_1) and the oligomer peaks makes it feasible to employ a ^{19}F NMR saturation transfer experiment to monitor the kinetics of ShaPrP(90−231) monomer−oligomer exchange within the β-state. As shown in Figure 6 for the WT sequence, there is a pronounced decay of the NMR signal arising from the oligomer peaks with increasing time of the saturation pulse

dx.doi.org/10.1021/ja404584s | J. Am. Chem. Soc. 2013, 135, 10533−10541

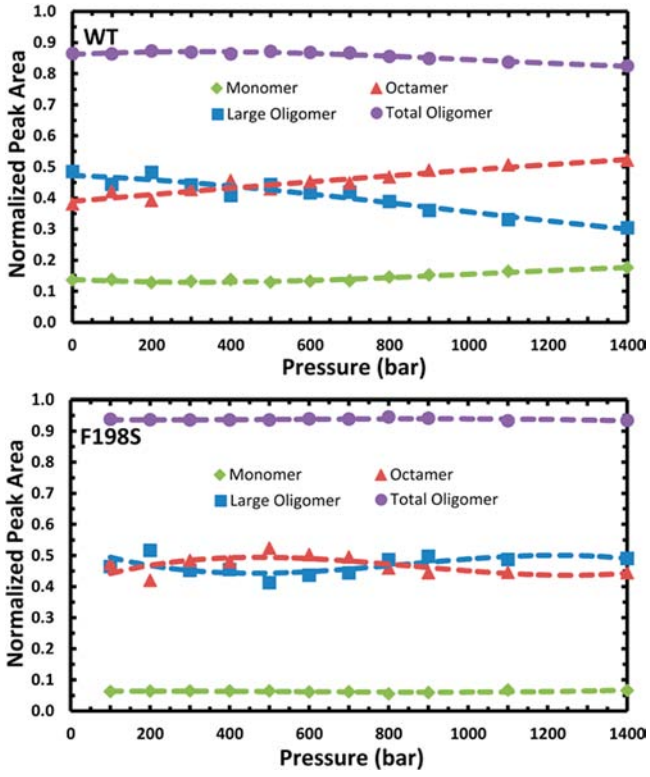

Figure 4. Normalized populations of monomeric and oligomeric ShaPrP(90−231)$^{\beta}$ as a function of pressure. The normalized peak areas obtained from deconvolution of ^{19}F spectra recorded as a function of pressure are shown for WT (top) and F198S (bottom) ShaPrP(90−231)$^{\beta}$. Peak fitting was performed for each sample as described in Figure 2. The total oligomer fraction represents the sum of the octamer and large oligomer populations. Curves are shown to guide the eye.

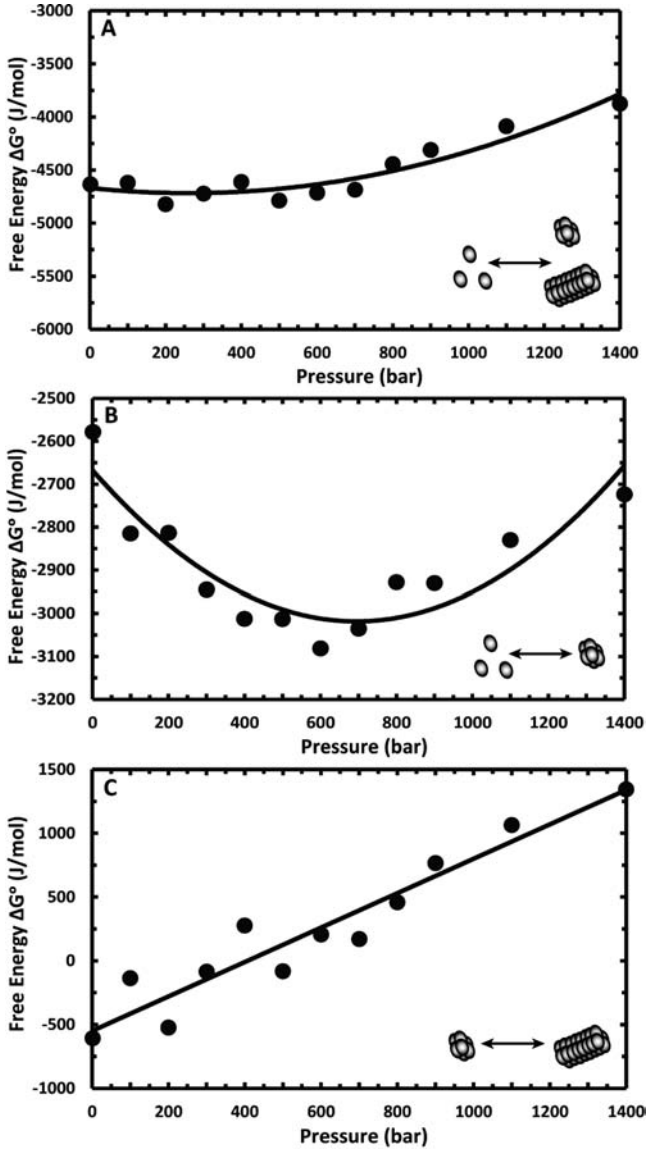

Figure 5. Equilibrium free energies associated with pressure-induced transitions in the oligomeric state of WT ShaPrP(90−231)$^{\beta}$. The free energies calculated for the monomer−oligomer (A), monomer to octamer (B), and octamer−large oligomer transitions (C) are shown as a function of pressure. Equation 4 was used to fit the experimental data.

selectively applied to the M_1 peak, while the other monomer peaks (M_2 and M_3) remain constant. A similar response is observed for the F198S mutant, as shown in Figure S3 in SI.

Fitting each decay profile to an equation corresponding to a two-state exchange model which incorporates the measured spin−lattice relaxation times of monomer and oligomer, and an exchange rate constant K, gave rate constants for monomer−total oligomer exchange of 0.15−0.20 Hz for both F198S and WT ShaPrP(90−231) (Table 2).[53] Deconvolution of the oligomer peak as described above allows estimation of the monomer−octamer and monomer−large oligomer exchange rates, giving 0.09−0.13 Hz and 0.23−0.25 Hz, respectively. While there is an additional source of error introduced by the deconvolution process, which is compounded by the presence of octamer−oligomer exchange, our results suggest a faster exchange of monomer with the larger oligomers than with the octamers.

Our kinetic analysis, based on the knowledge of the equilibrium constants, allows us to assemble both forward and reverse exchange rates. This is illustrated in Figure 7, which summarizes the estimated equilibrium populations and exchange rates between each of the three observed oligomeric states coexisting within the misfolded ShaPrP(90−231)$^{\beta}$. Consistent with a role for F198S mutation in stabilizing the β-octamer, the rate of dissociation of octamer to monomer is approximately 30% that of the WT protein. The reversibility of the temperature and pressure data and the lack of aggregation in our samples over extended timeframes (months) suggest that further perturbation, such as high salt or agitation, is required to promote fibril formation from the β-state. Therefore, only the three states identified above are presented in Figure 7.

DISCUSSION

The formation of intemediates along the misfolding pathway of PrP is well established and occurs in response to unfolding or destabilization of native PrP^{C} by temperature, pressure, or denaturant. Importantly the exact nature of the intermediate states is sensitive to the PrP sequence being studied and, in particular, to the solution conditions of the experiment. This has led to the identification of partially ordered monomeric folding intermediates[19−21,42] as well as β-sheet-rich oligomers.[21,22,26,36−40,59] While one report identifies a putative molten globule monomer with significant α-helical secondary

dx.doi.org/10.1021/ja404584s | J. Am. Chem. Soc. 2013, 135, 10533−10541

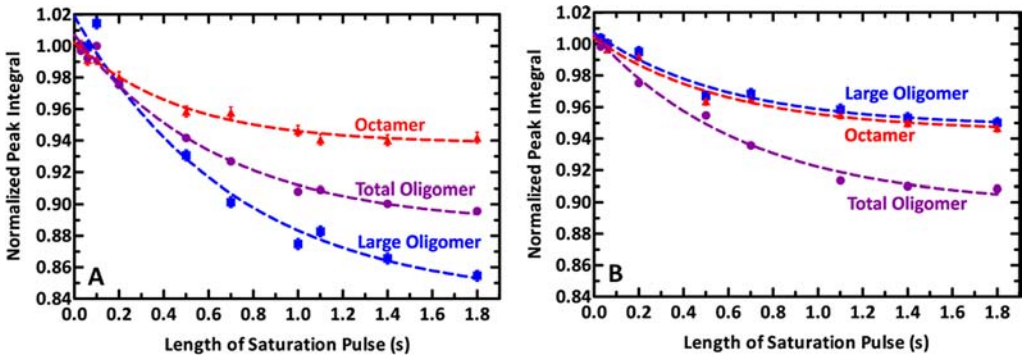

Figure 6. ^{19}F NMR saturation transfer measurements on ShaPrP(90−231)$^{\beta}$. Magnetization decay profiles of total oligomer (purple), octamer (red), and large oligomer (blue) components for WT ShaPrP(90−231)$^{\beta}$ (left) and F198S (right) after selective saturation of the M_1 β-monomer resonance for a series of mix times. No effective decay of the M_2 or M_3 β-monomer resonances (Figure S3) is observed. Control experiments, in which the saturation pulse was applied at an upfield frequency equidistant from the oligomer peaks, showed no signal decay. Here, k_{ex} and T_1 represent the fitting parameters associated with the decay profile. Error bars represent the RMS noise in the original spectra.

Table 2. Exchange Rate Constants Observed for WT and F198S ShaPrP(90−231)$^{\beta}$[a]

	WT		F198S	
	forward rate K_{ex} (s^{-1})	reverse rate K_{ex} (s^{-1})	forward rate K_{ex} (s^{-1})	reverse rate K_{ex} (s^{-1})
M−O	0.133 ± 0.012	0.032 ± 0.003	0.099 ± 0.012	0.009 ± 0.001
M−O	0.247 ± 0.025	0.043 ± 0.004	0.230 ± 0.040	0.0205 ± 0.0036
M−O+LO	0.187 ± 0.014	0.019 ± 0.001	0.159 ± 0.013	0.0072 ± 0.0006

[a]Forward and reverse rate constants are given for monomer (M)−octamer (O), monomer−large oligomer (LO), and monomer−total oligomer (O+LO) exchange, obtained by fitting the selective saturation data shown in Figure 6.

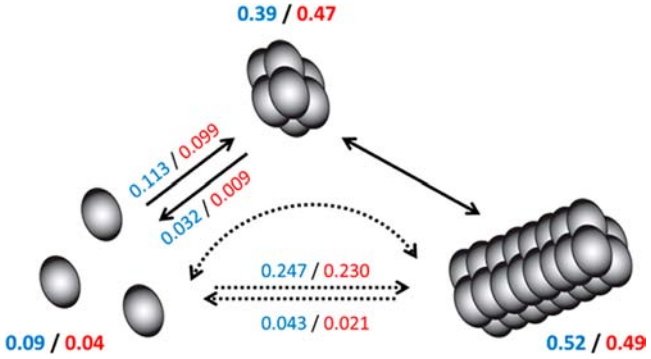

Figure 7. Model for equilibrium exchange between assembled states within ShaPrP(90−231)$^{\beta}$. The exchange processes at 28 °C and ambient pressure, observed between monomers, octamers, and larger oligomers of ShaPrP(90−231)$^{\beta}$ are indicated by arrows connecting the different species, with the corresponding rate constants (s^{-1}) and equilibrium populations (fraction of total, bold) given in blue (WT) and red (F198S mutant). The curved arrow indicates the possibility of monomer−oligomer exchange occurring only through an octameric intermediate, although our kinetic data support a direct addition of monomers to growing large oligomers.

structure,[21] the majority of the data in the literature supports the formation of non-native structures in the early stages of PrP unfolding or misfolding. In particular, several reports have shown that there is a minimum stable oligomer, generally identified as octameric, which is populated during misfolding of both full-length PrP and PrP(90−231).[21,22,26,36,37,39] While some groups claim this is a key intermediate populated on the pathway to fibrillization,[21,26,39] others suggest that these small oligomers are off-pathway intermediates, requiring dissociation and conformational rearrangement of the monomer before fibril assembly can take place.[22,37,38,47]

Irrespective of their potential role in formation of PrP^{Sc} or other amyloid fibrils, misfolding of PrP^{C} to cytotoxic β-sheet-rich assemblies remains important. The β-state intermediate in this study shares many features with reported β-sheet octamers and non-native monomers and has been shown to correlate with disease susceptibility and to exhibit cytotoxicity *in vitro*, making it a potentially important player in prion disease pathogenesis.[23,28] Additionally, the similarity of nonfibrillar PrP oligomers to those observed in amyloid and protein misfolding diseases[30,31,60] strongly suggests that an understanding of early events in PrP misfolding and assembly will also shed light on the mechanisms underlying the onset of these diseases.

Here we have examined the thermodynamic and kinetic parameters governing exchange between a misfolded monomer of ShaPrP(90−231), a relatively stable β-octamer, and a larger oligomer, using ^{19}F NMR, which is highly sensitive to chemical exchange and molecular dynamics. These misfolded states were populated under conditions previously shown to promote formation of a β-state ensemble containing non-native monomer and octamer in equilibrium.[23] Sokolowski et al. have also reported formation, under similar conditions of low pH and denaturant, of an ensemble of oligomers, with an octamer as the minimal stable size.[26]

Our thermodynamic analysis of the equilibria existing within the β-state support the concept that formation of a stable β-octamer represents a key step in assembly of misfolded PrP. The favorable entropic term and unfavorable enthalpy associated with oligomerization of the monomer (Table 1) is reminiscent of the energetics determining initiation of amyloid fibril formation, recently described by Buell et al.[61] Following this model, the enthalpic barrier to formation of oligomers is indicative of a loss of stable intramolecular contacts within the non-native monomer. The barrier is too low to prevent oligomer formation, likely due to the destabilizing conditions

under which the β-state is formed. Native intramolecular contacts have already been disrupted and replaced with a presumably less favorable set of interactions stabilizing a partially ordered non-native monomer.

Assembly from the monomeric intermediate is then entropically driven, suggesting a burial of hydrophobic groups that have been exposed following the loss of native structure and a concurrent desolvation of the oligomer. Formation of the larger oligomers is then enthalpically driven, suggesting that this process represents addition of octamers and monomers to a stable β-sheet core. We cannot rule out the possibility that conformational rearrangement is required for further assembly of the octamer into large oligomers, since the time scales involved are slow (seconds). Interestingly, exchange of monomer with the large oligomers occurs at a 3 to 4× higher rate than exchange with octamers, again supporting the notion of the octamer as a stable intermediate, whose formation may represent the rate-limiting step for assembly of misfolded PrP.

Our thermodynamic model is supported by both the significant decrease in heat capacity for the oligomeric states and by the pressure data, which suggest a more tightly packed structure relative to monomeric protein. It is important to note that the dissociation observed at increased pressures in our studies is consistent with previous investigations of PrP assembly under pressure.[38,45] Significantly higher pressures (~4000 atm) have been shown to reverse this trend, promoting aggregation. Similarly, at the temperatures used here, heating induces a dissociation of the large oligomer, favoring the octameric intermediate. Higher temperatures might be expected to promote higher-order aggregation, as suggested by our DLS data (Figure S1 in SI).

Overall, the model presented in Figure 7 is consistent with that of Sokolowski et al.,[26] as well as with the general models presented by Gerber et al.[21,39] The latter propose assembly of a putative decamer from a partially folded monomeric intermediate of human PrP(90−231), followed by subsequent stacking of these small oligomers into larger aggregates. Sokolowski et al. also present data suggesting that an octameric intermediate of ShaPrP(90−231) exists on-pathway to fibril formation, although fibrillization was extremely slow (55 days), and beyond the time scale of our current experiments. The kinetic data summarized in Figure 7 also suggest that formation of a stable small oligomer (i.e., β-octamer) from misfolded monomers may be a rate-limiting step in assembly, consistent with the concept that nucleation events are required to initiate the growth of amyloid fibrils *in vitro*. While the relationship of the β-state oligomers discussed here with assembly of amyloid fibrils or PrP^{Sc}-like structures remains unclear, the evidence for further assembly of the observed octamers into larger oligomers suggests the potential for nucleation of fibrillization. Further work will be required to define the on-/off-pathway nature of the β-state intermediates.

In addition to obtaining insight into the exchange between misfolded states for WT PrP(90−231), we examined the impact of a GSS-related mutation on the β-state ensemble. F198S is known to destabilize the native state of PrP, leading to spontaneous conversion to protease-resistant fibrils.[18] Apetri et al.[41] have previously demonstrated that certain prion disease related mutations can alter the denaturant folding kinetics of human PrP(90−231), promoting the formation of a partially folded (monomeric) intermediate. The F198S mutation in particular had the largest effect of the nine mutant proteins studied, leading to a 100x increase in the population of this folding intermediate in the absence of denaturant. Here, we report a significant decrease in the free energy associated with oligomer formation by the F198S mutant of ShaPrP(90−231), favoring formation of the octameric intermediate. This is the first indication that the F198S mutation may play a role in promoting assembly of misfolded PrP, in addition to its previously characterized role in destabilizing the native state. Our data also provide a proof-of-principle that examining the equilibria between misfolded states may shed light on the role of mutations and other sequence alterations in prion misfolding.

CONCLUSIONS

In conclusion, we have presented a detailed analysis of the thermodynamic and kinetic parameters governing the exchange between three distinct misfolding intermediates of ShaPrP(90−231). This supports an entropically driven assembly of an initial octameric structure, and provides some evidence for further assembly of this minimal unit into larger oligomers, through an enthalpically favorable process. Under the conditions used here, exchange between states is slow, occurring on the time scale of seconds. Surprisingly, a GSS-associated F198S mutation was found to promote oligomerization within the misfolded state, suggesting a dual role for this mutation in initiation of prion disease. Overall, our ^{19}F NMR approach has demonstrated the ability to obtain thermodynamic and kinetic parameters that define early aggregation events occurring during protein misfolding. This should be an increasingly useful tool for studying amyloid aggregation, especially when combined with recent developments in structural studies of nonfibrillar oligomers.

ASSOCIATED CONTENT

Supporting Information

^{19}F T_2 relaxation times and estimated line widths (Table S1), and analysis of the pressure-induced monomer−oligomer transitions (Table S2). DLS measurements (Figure S1), diffusion edited ^{19}F NMR spectra (Figure S2), and negative controls for the NMR saturation transfer experiments (Figure S3). This material is available free of charge via the Internet at http://pubs.acs.org.

AUTHOR INFORMATION

Corresponding Author

ssharpe@sickkids.ca; scott.prosser@utoronto.ca

Notes

The authors declare no competing financial interest.

ACKNOWLEDGMENTS

We thank Dr. Carlene Starck and Dr. Avi Chakrabartty for useful discussions. This work was funded by an operating grant to S.S. from PrioNet Canada. S.S. is a Canada Research Chairs Program chairholder (Tier II). R.S.P. acknowledges NSERC (Grant 261980) for a research discovery award.

REFERENCES

(1) Chiti, F.; Dobson, C. M. *Annu. Rev. Biochem.* **2006**, *75*, 333−366.
(2) Collins, S. J.; Lawson, V. A.; Masters, C. L. *Lancet* **2004**, *363*, 51−61.
(3) Collinge, J. *Annu. Rev. Neurosci.* **2001**, *24*, 519−550.
(4) Prusiner, S. B. *Science* **1982**, *216*, 136−144.
(5) Prusiner, S. B. *Bioessays* **1986**, *5*, 231.

(6) Donne, D. G.; VIles, J. H.; Groth, D.; Melhorn, I.; James, T. L.; Cohen, F. E.; Prusiner, S. B.; Wright, P. E.; Dyson, H. J. *Proc. Natl. Acad. Sci. U.S.A.* **1997**, *94*, 13452−13457.
(7) Liu, H.; Farr-Jones, S.; Ulyanov, N. B.; Llinas, M.; Marqusee, S.; Groth, D.; Cohen, F. E.; Prusiner, S. B.; James, T. L. *Biochemistry* **1999**, *38*, 5362−5377.
(8) Stahl, N.; Borchelt, D. R.; Hsiao, K.; Prusiner, S. B. *Cell* **1987**, *51*, 229−240.
(9) Caughey, B.; Lansbury, P. T. *Annu. Rev. Neurosci.* **2003**, *26*, 267−298.
(10) Cohen, F. E.; Prusiner, S. B. *Annu. Rev. Biochem.* **1998**, *67*, 793−819.
(11) McKinley, M. P.; Bolton, D. C.; Prusiner, S. B. *Cell* **1983**, *35*, 57−62.
(12) Pan, K. M.; Baldwin, M.; Nguyen, J.; Gasset, M.; Serban, A.; Groth, D.; Mehlhorn, I.; Huang, Z. W.; Fletterick, R. J.; Cohen, F. E.; Prusiner, S. B. *Proc. Natl. Acad. Sci. U.S.A.* **1993**, *90*, 10962−10966.
(13) Prusiner, S. B.; McKinley, M. P.; Bowman, K. A.; Bolton, D. C.; Bendheim, P. E.; Groth, D. F.; Glenner, G. G. *Cell* **1983**, *35*, 349−358.
(14) Horwich, A. L.; Weissman, J. S. *Cell* **1997**, *89*, 499−510.
(15) Castilla, J.; Saa, P.; Hetz, C.; Soto, C. *Cell* **2005**, *121*, 195−206.
(16) Hosszu, L. L.; Baxter, N. J.; Jackson, G. S.; Power, A.; Clarke, A. R.; Waltho, J. P.; Craven, C. J.; Collinge, J. *Nat. Struct. Biol.* **1999**, *6*, 740−743.
(17) Hosszu, L. L.; Wells, M. A.; Jackson, G. S.; Jones, S.; Batchelor, M.; Clarke, A. R.; Craven, C. J.; Waltho, J. P.; Collinge, J. *Biochemistry* **2005**, *44*, 16649−16657.
(18) Vanik, D. L.; Surewicz, W. K. *J. Biol. Chem.* **2002**, *277*, 49065−49070.
(19) Apetri, A. C.; Surewicz, W. K. *J. Biol. Chem.* **2002**, *277*, 44589−44592.
(20) Martins, S. M.; Chapeaurouge, A.; Ferreira, S. T. *J. Biol. Chem.* **2003**, *278*, 50449−50455.
(21) Gerber, R.; Tahiri-Alaoui, A.; Hore, P. J.; James, W. *J. Biol. Chem.* **2007**, *282*, 6300−6307.
(22) Baskakov, I. V.; Legname, G.; Baldwin, M. A.; Prusiner, S. B.; Cohen, F. E. *J. Biol. Chem.* **2002**, *277*, 21140−21148.
(23) Khan, M. Q.; Sweeting, B.; Mulligan, V. K.; Arslan, P. E.; Cashman, N. R.; Pai, E. F.; Chakrabartty, A. *Proc. Natl. Acad. Sci. U.S.A.* **2010**, *107*, 19808−19813.
(24) Redecke, L.; von Bergen, M.; Clos, J.; Konarev, P. V.; Svergun, D. I.; Fittschen, U.; Broekaert, J. A. C.; Bruns, O.; Georgieva, D.; Mandelkow, E.; Genov, N.; Betzel, C. *J. Struct. Biol.* **2007**, *157*, 308−320.
(25) Silveira, J. R.; Raymond, G. J.; Hughson, A. G.; Race, R. E.; Sim, V. L.; Caughey, B. *Nature* **2005**, *437*, 257−261.
(26) Sokolowski, F.; Modler, A. J.; Masuch, R.; Zirwer, D.; Baier, M.; Lutsch, G.; Moss, D. A.; Gast, K.; Naumann, D. *J. Biol. Chem.* **2003**, *278*, 40481−40492.
(27) Vendrely, C.; Valadie, H.; Bednarova, L.; Cardin, L.; Pasdeloup, M.; Cappadoro, J.; Bednar, J.; Rinaudo, M.; Jamin, M. *Biochim. Biophys. Acta* **2005**, *1724*, 355−366.
(28) Simoneau, S.; Rezaei, H.; Sales, N.; Kaiser-Schulz, G.; Lefebvre-Roque, M.; Vidal, C.; Fournier, J.-G.; Comte, J.; Wopfner, F.; Grosclaude, J.; Schatlz, H.; Lasmezas, C. I. *PLoS Pathog.* **2007**, *3*, 1175−1186.
(29) Kazlauskaite, J.; Young, A.; Gardner, C. E.; Macpherson, J. V.; Venien-Bryan, C.; Pinheiro, T. J. *Biochem. Biophys. Res. Commun.* **2005**, *328*, 292−305.
(30) Glabe, C. G. *Neurobiol. Aging* **2006**, *27*, 570−575.
(31) Kayed, R.; Head, E.; Thompson, J. L.; McIntire, T. M.; Milton, S. C.; Cotman, C. W.; Glabe, C. G. *Science* **2003**, *300*, 486−489.
(32) Krishnan, R.; Goodman, J. L.; Mukhopadhyay, S.; Pacheco, C. D.; Deniz, A. A.; Lindquist, S. *Proc. Natl. Acad. Sci. U.S.A.* **2012**, *109*, 11172−11177.
(33) Ono, K.; Condron, M. M.; Teplow, D. B. *Proc. Natl. Acad. Sci. U.S.A.* **2009**, *106*, 14745−14750.
(34) Baglioni, S.; Casamenti, F.; Bucciante, M.; Luheshi, L. M.; Taddei, N.; Chiti, F.; Dobson, C. M.; Stefani, M. *J. Neurosci.* **2006**, *26*, 8160−8167.
(35) Bucciantini, M.; Giannoni, E.; Chiti, F.; Baroni, F.; Formigli, L.; Zurdo, J.; Taddei, N.; Ramponi, G.; Dobson, C. M.; Stefani, M. *Nature* **2002**, *416*, 501−511.
(36) Baskakov, I. V.; Legname, G.; Prusiner, S. B.; Cohen, F. E. *J. Biol. Chem.* **2001**, *276*, 19687−19690.
(37) Bocharova, O. V.; Breydo, L.; Parfenov, A. S.; Baskakov, I. V. *J. Mol. Biol.* **2005**, *346*, 645−659.
(38) El Moustaine, S.; Perrier, V.; Smeller, L.; Lange, R.; Torrent, J. *FEBS J.* **2008**, *275*, 2021−2031.
(39) Gerber, R.; Voitchovsky, K.; Mitchel, C.; Tahiri-Alaoui, A.; Ryan, J. F.; Hore, P. J.; James, W. *J. Mol. Biol.* **2008**, *381*, 212−220.
(40) Lu, B. Y.; Chang, J. Y. *Biochem. J.* **2002**, *364*, 81−87.
(41) Apetri, A. C.; Surewicz, K.; Surewicz, W. K. *J. Biol. Chem.* **2004**, *279*, 18008−18014.
(42) Torrent, J.; Alzarez-Martinez, M. T.; Heitz, F.; Liautard, J.-P.; Balny, C.; Lange, R. *Biochemistry* **2003**, *42*, 1318−1325.
(43) Bjorndahl, T. C.; Zhou, G.-P.; Liu, X.; Perez-Pineiro, R.; Semenchenko, V.; Saleem, F.; Acharya, S.; Bujold, A.; Sobsey, C. A.; Wishart, D. S. *Biochemistry* **2010**, *50*, 1162−1173.
(44) Tahiri-Alaoui, A.; Sim, V. L.; Caughey, B.; James, W. *J. Biol. Chem.* **2006**, *281*, 34171−34178.
(45) Torrent, J.; Alzarez-Martinez, M. T.; Liautard, J.-P.; Balny, C.; Lange, R. *Protein Sci.* **2005**, *14*, 956−967.
(46) Hsiao, K.; Baker, H. F.; Crow, T. J.; Poulter, M.; Owen, F.; Terwilliger, J. D.; Westaway, D.; Ott, J.; Prusiner, S. B. *Nature* **1989**, *338*, 342−345.
(47) Baskakov, I. V.; Legname, G.; Gryczynski, Z.; Prusiner, S. B. *Protein Sci.* **2004**, *13*, 586−595.
(48) Corsaro, A.; Paludi, D.; Villa, V.; D'Arrigo, C.; Chiovitti, K.; Thellung, S.; Russo, C.; Di Cola, D.; Ballerini, P.; Patrone, E.; Schettini, G.; Aceto, A.; Florio, T. *Int. J. Immunopathol. Pharmacol.* **2006**, *19*, 339−356.
(49) Corsaro, A.; Thellung, S.; Villa, V.; Nizzari, M.; Aceto, A.; Florio, T. *Omics: J. Integr. Biol.* **2012**, *16*, 50−59.
(50) Gerig, J. T. *Prog. Nucl. Mag. Reson. Spectrosc.* **1994**, *26*, 293−370.
(51) Kitevski-LeBlanc, J. L.; Prosser, R. S. *Prog. Nucl. Mag. Reson. Spectrosc.* **2012**, *62*, 1−33.
(52) Kitevski-LeBlanc, J. L.; Evanics, F.; Prosser, R. S. *J. Biomol. NMR* **2010**, *48*, 113−121.
(53) Helgstrand, M.; Hard, T.; Allard, P. *J. Biomol. NMR* **2000**, *18*, 49−63.
(54) Stejskal, E.; Tanner, J. *J. Chem. Phys.* **1965**, *42*, 288−292.
(55) Park, C.; Marqusee, S. *Protein Sci.* **2004**, *13*, 2553−2558.
(56) Seewald, M. J.; Pichumani, K.; Stowell, C.; Tibbals, B. V.; Regan, L.; Stone, M. J. *Protein Sci.* **2000**, *9*, 1177−1193.
(57) Tanner, J. E. *J. Chem. Phys.* **1970**, *52*, 2523−2526.
(58) Abragam, A. *The Principles of Nuclear Magnetism*; Claredon Press: Oxford, 1961.
(59) Eghiaian, F.; Daubenfeld, T.; Quenet, Y.; van Audenhaege, M.; Bouin, A.-P.; van der Rest, G.; Grosclaude, J.; Rezaei, H. *Proc. Natl. Acad. Sci. U.S.A.* **2007**, *104*, 7414−7419.
(60) Walsh, P.; Sharpe, S. In *Neurodegenerative Diseases, Book 2*; Chang, R. C.-C., Ed.; InTech Open Access Publisher : New York, 2011.
(61) Buell, A. K.; Dhulesia, A.; White, D. A.; Knowles, T. P. J.; Dobson, C. M.; Welland, M. E. *Angew. Chem., Int. Ed.* **2012**, *51*, 5247−5251.